Annuaire de l'Université "St. Kliment Ohridski", Faculté de Physique, 99, 2006

THE ATTENUATED TOTAL INTERNAL REFLECTION AS A BASIS FOR SOME SENSOR TECHNIQUES: AN INTERFEROMETRIC APPROACH

HRISTIYAN STOYANOV

Department of Quantum Electronics

Християн Стоянов. НАРУШЕНОТО ПЪЛНО ВЪТРЕШНО ОТРАЖЕНИЕ КАТО ОСНОВА НА НЯКОИ ИЗМЕРИТЕЛНИ МЕТОДИ: ИНТЕРФЕРОМЕТРИЧЕН ПОДХОД

Поради големите потенциални възможности за полезни приложения, явлението нарушено пълното вътрешно отражение е обект на непрестанен интерес. В настоящата статия е описан прост интерфометричен метод за измерване на малки разстояния между две равнинни граници на среди. Разгледани са теоретично и експериментално поляризационните ефекти, съпровождащи този процес. Методът се базира на интерферометрично възстановяване на *p*- и *s*-компонентите на отразеното поле. От интерференчния сигнал се определя фазовото отместване между тях. При експериментите бе наблюдавано напречно отместване на ивиците и вариации на разпределението на интензитета. Във втората част на работата е предложена проста теория, обясняваща този ефект. За тази цел е изведена взаимната връзка между интерферометричния сигнал и поляризационното състояние на полето, представено с неговия вектор на Стокс. Направено е сравнение между теоретичните и експерименталните резултати.

Hristiyan Stoyanov. THE ATTENUATED TOTAL INTERNAL REFLECTION AS A BASIS FOR SOME SENSOR TECHNIQUES: AN INTERFEROMETRIC APPROACH

The attenuated total internal reflection (ATIR) is an area of constant interest. The reason for that is the great variety of useful applications based on this phenomenon. In this paper we describe a simple interferometric phasemeter which can be used as a proximity sensor. The polarization effects accompanying the process are also discus theoretically and experimentally. This method is based on the interferometric restoration of both *p*- and *s*-components of the resultant field. The phase shift between them as a function of the attenuation of the total internal reflection can be determined from the interference signal. An experimental effect of

lateral fringe shift and variations in intensity distribution of the interferometrical signal was observed during the measurements by an angular sheering polarization interferometer. In the second part of this work a simple theory is proposed to explain these effects. For that reason the relationship between the polarization effects, accompanying the ATIR and the output interferometrical signal had to be taken into account. To explain the variations of interference fringes intensity topography, the evolution of the Stokes parameters as a function of the gap width for Si attenuator is studied numerically.

Keywords: interferometry, TIR, polarization, linear measurements
PACS numbers: 42.25.Fx, 42.25.Gy, 42.25.Hz, 73.20.Mf

1. INTRODUCTION

The total internal reflection (TIR) is an area of constant interest. The reason for that is the great variety of useful applications based on this phenomenon. Attenuated TIR (ATIR) can be used for creating fixed or variable phase retarders [1–3, 6], variable filters [4], in refractometry of optical materials such as absorbing liquids [14], metals, biotissue [5], for investigation of surface relief [15], etc. A number of papers devoted to the near field scanning optical microscopy are connected with the application of TIR for investigation of surface properties of various media [see e.g. 7]. Many experimental works in this field, mainly in the region of the longer wavelengths (infrared [1] and microwaves [11]) have been carried out so far. The small values of the wavelengths in visible make the investigations of the amplitude and phase changes during the processes of attenuating TIR difficult. On the other hand, the interferometers as precise measuring tools give us the possibility to bring up the research at higher level of accuracy. Interferometry in the visible region is a well established and highly developed method covering very large area of applications (see e.g. [19, 20]). For example, Nakadate [16–18] described a method using a polarization interferometer for precise detection of the mean phase of interferometric pattern that consists equidistant and straight fringes.

In the present paper a very simple method for restoration of both *p*- and *s*-components of ATIR field is presented, and the phase shift between these is investigated. An application for proximity sensing is described as well. In contrast to Nakadate's work, this paper is devoted on the investigation of the local phase-variations. The measurement is concentrated on restricted spatial range, covering approximately one fringe. The rest of the interference pattern is a basis for comparison.

2. A POLARIZATION INTERFEROMETER FOR PROXIMITY SENSING

2.1. THE OPTICAL SETUP

Following the classical way of study of the process of TIR [12] we regard the incident and the output fields as compositions of two independent fields: the *p*- and *s*-components. A plane monochromatic wave falling on the plane boundary between two media, the first of which is denser and the second one is rarer, is totally reflected, if the angle of incidence is grater than the critical one. The both components, *p*- and *s*-, are reflected without amplitude losses but they are phase shifted [12]. Placing a third medium in the proximity of the plane boundary leads to the so called attenuating of the TIR, which means that not only phase shifts but also amplitude losses of both components will be observed. To study this phenomenon we need a device which allows us to extract from the reflected wave both, *p*- and *s*-components and to let them interfere in a certain way. This two components have to be with minimum distortions. This is difficult to be achieved because of the influence of the inhomogenities of the media and imperfectness of the boundaries the wave is passing through. One possible solution of this problem is to use a polarization beamsplitter followed by a linear polarizer (see Fig. 1). These elements compose a simple shearing interferometer which can be used to study either the phase shifts between these two components or the amplitude changes.

The basic idea is to adjust the plane of incidence of the TIR prism to contain the two rays at the exit of the beam splitter. If we use a crystal beam splitter, the construction is simplified when the plane of incidence in the TIR prism coincides with a plane of crystal symmetry (the *p*- *s*-vector basis coincides with the local coordinate system of the beamsplitting prism). Then the two refracted by the beamsplitting prism rays lie in a single plane. This happens when the plane of incidence either contains the optical axis of the crystal or is perpendicular to it. This condition is fully fulfilled for polarization beamsplitters like Wollaston, Rochon or Senarmont prisms [21]. The exit ordinary and extraordinary rays correspond to *p*- and *s*-components of the ATIR field, depending on the type of the beamsplitting prism we use. The advantage of this arrangement is that it preserves the original values of both components (*p*- and *s*-) of the ATIR field with minimum distortion. After some further modification such an optical system could be included in proximity sensors, or be used for surface geometry control, for variable optical retarders, contamination monitoring, etc.

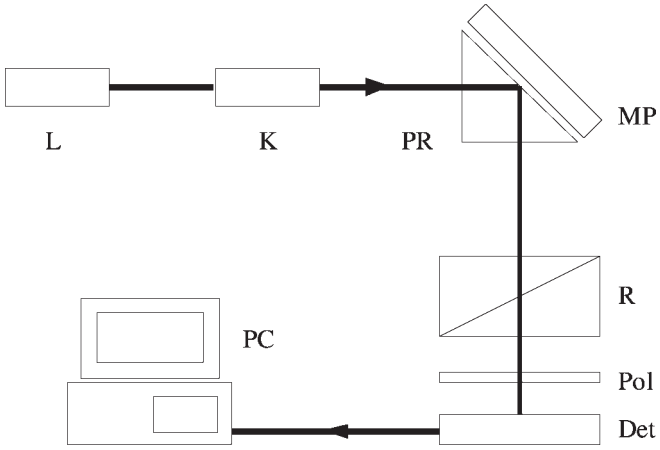

Fig. 1. Sketch of the equipment: L – laser source; K – collimator; PR – TIR glass prism; MP – metal plate; R – Rochon prism; Pol – linear polarizer; Det – photodiode array detector; PC – personal computer with a framegraber

The optical system used in the experiment is shown in Fig. 1. It consists of a laser source L of linearly polarized light, which is expanded and collimated by the collimator K. The plane wave so obtained propagates through the TIR prism PR and the shearing interferometer consisting of a polarization beamsplitter R and a linear polarizer Pol. The interferometric fringes are detected by an image array sensor Det and analysed by a PC–AT compatible computer. All elements are mounted on a vibration-isolated optical table.

A detailed view of the interferometer is shown in Fig. 2. It is a common path polarization shearing interferometer. The coordinate system is oriented so that the z axis is along the direction of propagation of the laser beam and the x axis is in the plane of incidence. As a polarization beamsplitter was used a quartz Rochon prism. Compared with the Wollaston prism (which can be used too), the Rochon prism gives smaller value of the angular shear β. It also preserves the direction of propagation of the incident wave (for the ordinary wave, which coincides with the p-component of the TIR field). This proved to be an advantage in the process of aligning of the optical system.

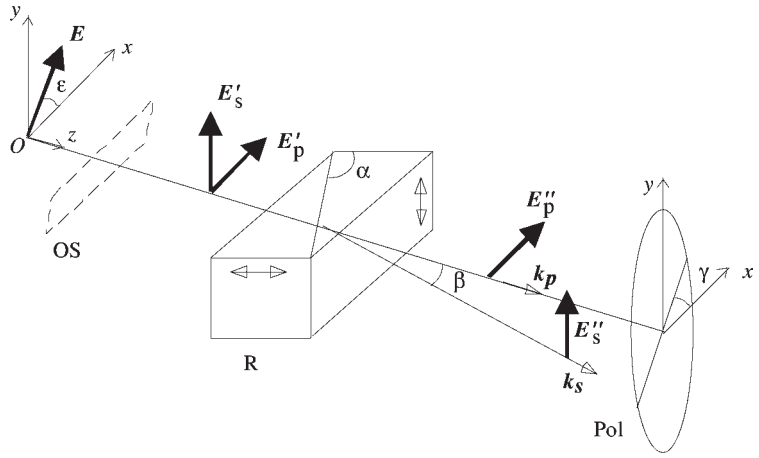

Fig. 2. The geometry of the interferometer: *Oxyz* – the laboratory coordinate system; OS – ATIR system oriented so that *x* and *z* are in the plane of incidence, and *y* is normal to it; R – Rochon prism oriented so that the optical axis of the first quartz prism is parallel to *z* and the optical axis of the second prism is parallel to *y*. In this case the angular shift β is in the plane of incidence. Pol – linear polarizer at azimuthal angle γ

The field vector $\boldsymbol{E}$ at the entrance pupil of the optical system OS to be studied (the TIR prism with a metal plate MP acting as attenuater) subtends an azimuth angle ε with the plane of incidence. At the exit pupil of OS the electric field, represented by its Jones vector, is given by [13]:

$$\begin{bmatrix} E'_p \\ E'_s \end{bmatrix} = \begin{bmatrix} r_0 & 0 \\ 0 & r_s \end{bmatrix} \begin{bmatrix} E_p \\ E_s \end{bmatrix}, \tag{1}$$

where $E_p = |\boldsymbol{E}| \cos\varepsilon$ and $E_s = |\boldsymbol{E}| \sin\varepsilon$ are the components of the entrance Jones vector (for the *p*- and *s*-polarization, respectively). The complex amplitude reflection coefficients are written as:

$$r_p = \rho_p \exp\left(i\delta_p\right), \tag{2}$$

$$r_s = \rho_s \exp\left(i\delta_s\right). \tag{3}$$

In the experimental part of this work the phase difference between the two components ($\Delta = \delta_p - \delta_s$) is studied. This was carried out by analysing the fringe pattern at the exit of the interferometer. The expressions for calculating r_p and r_s, derived on the basis of the theory of stratified optical media are [8, 9], are

$$r_s = \frac{Z_{0s}^i (A - CZ_{0s}^f) + (B - AZ_{0s}^f)}{Z_{0s}^i (A + CZ_{0s}^f) + (B + AZ_{0s}^f)}, \tag{4}$$

$$r_p = \frac{Z_{0p}^i (CZ_{0p}^f - A) + (AZ_{0p}^f - B)}{Z_{0p}^i (CZ_{0p}^f + A) + (AZ_{0p}^f + B)}, \tag{5}$$

where the indices *i* and *f* refer to the initial and final media, respectively. *A*, *B*, *C* are the elements of the transmission matrix through the gap with thickness *h*

$$\begin{bmatrix} A & B \\ C & A \end{bmatrix} = \begin{bmatrix} \cosh \alpha_2 h & Z_{0,2} \sinh \alpha_2 h \\ Z_{0,2}^{-1} \sinh \alpha_2 h & \cosh \alpha_2 h \end{bmatrix}, \tag{6}$$

where $\alpha_2 = k(n_3^2 \sin^2\theta_3 - 1)^{1/2}$.

The characteristic boundary impedance $Z_{0,2}$ is defined as

$Z_{0,2} = (\cos\theta_2)^{-1}$ for *s*-polarization, and

$Z_{0,2} = (\cos\theta_2)$ for *p*-polarization.

Also, $\cos\theta_2 = -i(n_3^2 \sin^2\theta_3 - 1)^{1/2}$ gives the direction of propagation of the wave in the rarer medium (in our case air). The characteristic boundary impedances of the initial and final media are given by

$$Z_{0,s}^i = [(n_1 - i\kappa_1)\cos\theta_1]^{-1}, \quad Z_{0,s}^f = (n_3 \cos\theta_3)^{-1}, \tag{7}$$

$$Z_{0,p}^i = (n_1 - i\kappa_1)^{-1} \cos\theta_1, \quad Z_{0,p}^f = n_3^{-1} \cos\theta_3, \tag{8}$$

where

$$\sin\theta_1 = (n_3 \sin\theta_3)/(n_1 - i\kappa_1),$$

$$\cos\theta_1 = (1 - \sin^2\theta_1)^{1/2}, \ \mathrm{Re}(\cos\theta_1) > 0,$$

n_3 is the index of refraction of the glass prism PR (see Fig. 1). $N_1 = n_1 - ik_1$ is the complex index of refraction of the bulk absorbing medium MP. The angles θ_1 and θ_3 give the directions of propagation of the wave in the absorbing medium and in the glass prism, respectively. We assume a plane wave falling from the side of the denser media (the prism PR) on the plane boundary with the rarer one. For angles of incidence θ_3 near to or exceeding the critical angle of TIR, the complex coefficients of amplitude reflection for both *p*- and *s*-components of the incident field depend on the boundary conditions. This conditions, (presented by the characteristic boundary impedances) depend on the optical properties of the attenuator, inserted in the less dense medium in the proximity of the boundary.

If the detector (see Fig. 1) is a linear photodiode array oriented along the

x axis, the measured fringe intensity can be written in the form:

$$I(x) = I_0 \cos^2(\varepsilon)\cos^2(\gamma)\left\{\rho_p^2 + \rho_s^2 tg^2(\gamma) + \right.$$
$$\left. +2\rho_p\rho_s tg(\varepsilon)tg(\gamma)\cos\left[\Phi(x,\Delta)\right]\right\},$$

where:

$$\Phi(x,\Delta) = \left(\boldsymbol{k}_p - \boldsymbol{k}_s\right)\cdot\boldsymbol{r} + \frac{2\pi}{\lambda}d(x)\left[n_0 - \frac{n_e(\beta)}{\cos(\beta)}\right] + \Delta\,, \tag{9}$$

where $\Delta = \delta_p - \delta_s\beta$ is the angle deviation between the ordinary and the extraordinary rays at the exit of the Rochon prism; γ is the azimuth of the polarizer; $d(x)$ is the current thickness of the second right angle prism of the Rochon prism; $\boldsymbol{r}$ is the radius vector of the point of measurement. In our case it lays in 0xz plane; $\boldsymbol{k}_p, \boldsymbol{k}_s$ are the wave vectors of the ordinary and extraordinary waves, which are corresponding to the p- and s-components of the ATIR field, respectively.

The first two terms in Eq. (9) form the carrier frequency of the interferometric signal. For a plane wave this signal represents a family of straight parallel fringes. The third term ($\Delta = \delta_p - \delta_s$) in (9), which is a function of additional physical and geometric parameters leads to a distortion of the basic set of fringes, provided the azimuth angles ε and γ are kept constant.

From the expressions for r_p and r_s, it is clear that ρ_p, ρ_s and Δ depend on gap thickness h, on the angle of incidence, and on the optical properties of the various media the wave is passing through. The theoretical investigation of the h-dependence of ρ_p, ρ_s shows that this dependence is not as strong and it can be neglected in the first approximation. Nevertheless, finer contrast measurements can provide an additional useful information. Also, if the azimuth angles ε and γ are variable it would be possible to study either the p- or the s-properties of the system.

2.2 EXPERIMENT

The source of linearly polarized coherent light in Fig. 1 is a HeNe laser (Melles Griot, 3 mW), working in TEM_{00} mode. The beam is expanded and collimated up to approximately 50 mm dia by a well corrected collimator (Jodon, model BET-50 with 10μm pin hole spatial filter). From the so generated plane wave only a small part was used–approximately 2 × 15 mm in the central area of the aperture. The plane wave propagates through the TIR prism PR which was made of optical glass with N = 1.56687 at λ = 632.8 nm. The polarization interferometer consists of a crystal quartz Rochon prism and sheet linear polarizer. The Rochon prism is a composition of two thin wedges.

In this way we obtain angular shear β of about 1.77×10^{-4} rad so that only four fringes (the basic 'carrier' interference pattern) cover the full aperture of the sensor. The photodiode array image sensor (Matsushita, model MN-512K) with 512 elements was used to detect photometric sections trough the interferometric fringes. The pixel dimensions of the sensor are 28×16 μm and the pitch is 28 μm. The total length of the sensitive area is 14.3 mm. The analog-to-digital converter of the slot card framegraber provides 8 bit quantization of the video signal. The scanning time can be programmed from 4 ms to 16 s. The scan accumulator allows up to 32 767 scans to be averaged. Special attention has been paid to the measurement of the gap width *h*. This was carried out by following visually the displacement of the white light coloured fringes localized in the gap by means of measuring microscope (not shown in Fig. 1) with long working distance lens (about 122 mm). The white light Fizeau fringes were observed in direction approximately normal to the hypotenuse of the TIR prism. To accomplish the *h*-movement a kinematic homemade support, holding the attenuater was used. This support consists of a system of tree point micro-screw adjusting stage and piezotransducer on it. On the top of the transducer the sample was fixed by spirituous solution of shellac. The sample manipulated by the three micro-screws and the transducer was adjusted up to almost parallel position against the glass plane of the TIR prism. The area of the sample was adjusted to get in contact with the plane of the prism. From this initial situation the sample was rotated step by step around a vertical axis and the movement and the width of the dark brown-yellow fringe (λ = 419 nm approximately) was registered by the microscope. Only one fringe from the basic pattern was affected by ATIR (see Fig. 3). Additional correction of the values of *h* due to the influence of through–the prism observation was carried out. The range of variation of the values of *h* was chosen to be less than 300 nm (an interval approximately equal to $\lambda/2$). The reason for this was to avoid the ambiguity connected with the change of the phase sign.

The results of the experiment are shown in Fig. 3 and Fig. 4. Fig. 3 shows four photometric sections carried out with the array detector trough the straight interferometric fringes. When the gap width *h* varies, ATIR in the region of the third fringe (counted from left to right) is observed. The *x* coordinate on the plot is in the plane of the sensor and is orientated along the array of photodiode pixels. The azimuth angles ε and γ, and the angle of incidence θ_3 were adjusted to be 45°. The phase shift in the first diagram (Fig. 3a) was measured for $h = 0$ and phase shift Δ was determined to be $-\pi$ radians. The next three diagrams (Fig. 3b, c, d) show phase shifts of –2.45, –1.08 and 0 radians for h = 16 nm, 69 nm, 156 nm, respectively. ATIR was

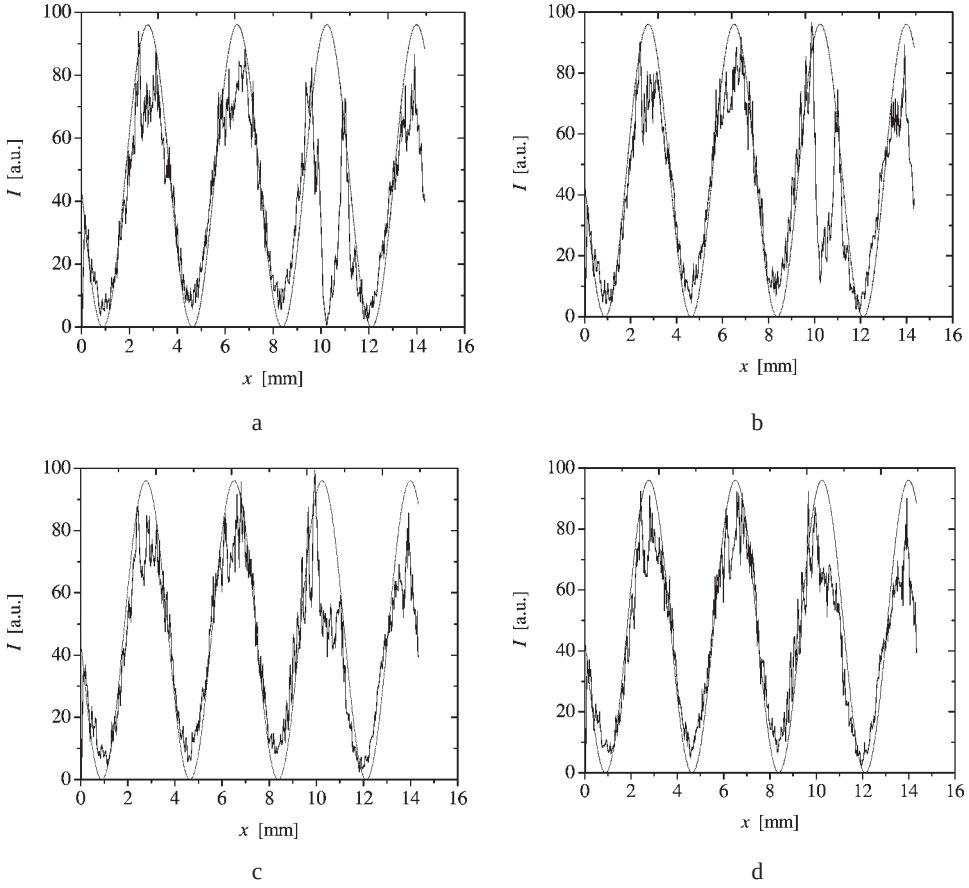

Fig. 3. Photometric sections trough the interferometric fringes obtained from the image sensor .The sample is a bulk polished plate of Si mono-crystal for: a) h = 0; b) h = 16 nm; c) h = 69 nm; d) h = 156 nm. The ATIR affects only the third fringe. Doted curve is the ideal noiseless signal as a reference

obtained by inserting a small sample of a bulk polished plate of silicon mono-crystal, N-type, cut at (1,0,0) (N_1 = 3.85 – i0.02 at λ = 632.8nm [10]).

The theoretical and experimental results are shown in Fig. 4. There is a good agreement between the predicted and the measured values near the contact. With rising h progressive discrepancy between theory and experiment is observed. That could be a result of the surface curvature or of some oxidation of the sample.

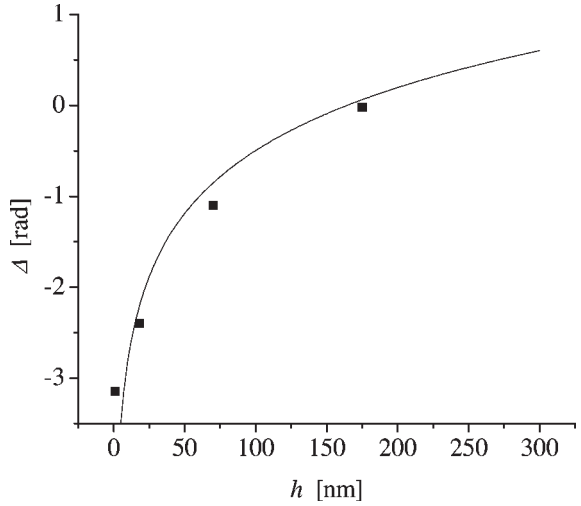

Fig. 4. Phase shift $\Delta = \delta_p - \delta_s$ as a function of the gap thickness h: comparison between the theoretic curve (solid line) and the experimental results

3. THE ROLE OF THE POLARIZATION IN ATIR PROXIMITY SENSING

Proximity sensing, based on the ATIR, as described in Section 2, is a precise interferometrical measurement, in the course of which strong changes of the polarization state of the initial wave could be observed. Further measurements showed that this phenomena lead to significant variations in the spatial intensity distribution of the interferometrical signal. To analyze and explain the behavior of the output signal, the polarization transforming mechanism has to be taken into consideration.

The polarization state of the light fields is fully described by the Stokes parameters. Being a versatile instrument for polarization investigations, the Stokes parameters are used in very wide spectral range–from radio polarimetry [23] down to UV [24] and X-ray [25] wavelengths, as well as in nonlinear optics [30]. The evolution of the Stokes parameters has been studied recently in different area of the optical measurements. Many papers are devoted to the influence of the anisotropic media, including liquid crystals, on the light wave [10, 30, 31].

In Section 2 we pointed out that the dependence of the modulus of the reflectivities for *p*- and for *s*-polarizations on the gap width is not as strong and can be neglected in the first approximation. Nevertheless, finer contrast measurements proved that this assumption is not well fulfilled, especially for

lower values of the gap width. The explanation can be found in the strong changes of the state of polarization–a process, accompanying the ATIR.

The purpose of the present discussion is to explain the role of the polarization in the simultaneous effects of intensity degradation and lateral shift of the interference fringes. As will be demonstrated, there is a great dynamics in the behavior of the Stokes parameters when the gap width varies. This process is not so simple to be explicitly described. For this purpose a simple analytical model of the relationship between the interferometrical signal intensity and the polarization state had to be build. The interferometrical signal is expressed in terms of the Stokes parameters, which are function of the gap width and of the optical properties of all media. We study numerically the evolution of the Stokes parameters as a function of the gap width for silicon attenuator. As a consequence, the evolution of the interferometrical signal, obtained by an angular sheering polarization interferometer, is also described and compared with the experimental data.

3.1. A BRIEF THEORY OF THE INTERFEROMETER

The optical setup (Fig. 5) is similar to that described in Section 2. Our experiment consists again of a TIR right angle prism, attenuating plate and an angular shearing interferometer in series. The attenuated totally reflected

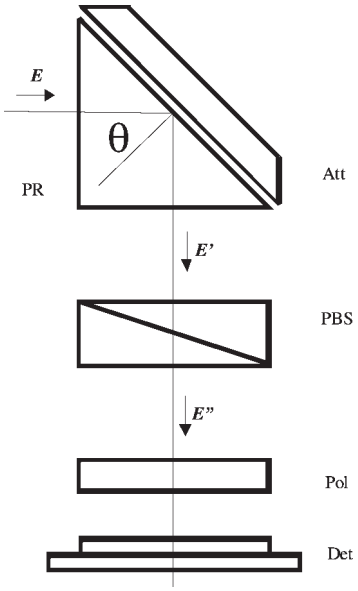

Fig. 5. Sketch of the optical setup: PR – TIR glass prism; Att – attenuator; PBS – polarizing beam splitter (Rochon prism); Pol – linear polarizer; Det – photodiode array detector

field is analyzed by means of the interferometer, which consists of a polarizing beam splitter (PBS), in our case a Rochon prism, a linear polarizer acting as analyzer, and a photodiode linear array.

During the measurements by means of this device we observed an effect of lateral fringe shift and variations in intensity distribution of the interferometrical signal, especially for gap widths smaller than half a wavelength. The aim of the hereafter-described simple theoretical model is the explanation of this phenomenon.

The polarization state of the ATIR field depends on the separation h between the dielectric boundary and the surface of the attenuator. This relationship is highly nonlinear and affects both the amplitude and the phase of each component (p- or s-) of the totally reflected field. The intensity distribution of the interferometrical signal is very sensitive to small changes of the amplitudes and phases [19]. As in our work we consider monochromatic light, both these parameters directly define the polarization state of the wave. The time averaging used below is just for correctness. To express the dependence of the fringe intensity distribution, obtained in the exit pupil of our interferometer, on the polarization state of the ATIR wave, we will rewrite the low of two-wave interference in terms of the Stokes parameters of that field.

The coordinate system is oriented so that x axes lies in the plane of incidence, y axes is orthogonal to it and z axes to be along the direction of propagation of the light. For all vector components, considered below, holds $p \equiv x$ and $s \equiv y$. The wave intensity and its state of polarization are completely determined by the elements of the coherence matrix $\boldsymbol{J}$, i.e. the autocorrelations $J_{ii} = \langle E_i^* E_i \rangle$ and the cross correlations $J_{ij} = \langle E_i^* E_j \rangle$ of the field components. In this expressions, the asterisk denotes complex conjugate, $\langle\rangle$ means time averaging and ($i, j = x, y$).

The complex amplitudes in the input and output of the ATIR prism, respectively,

$$\boldsymbol{E} = \begin{bmatrix} E_x \\ E_y \end{bmatrix}, \quad \boldsymbol{E}' = \begin{bmatrix} E'_x \\ E'_y \end{bmatrix}, \tag{10}$$

are related by

$$\boldsymbol{E}' = \boldsymbol{T}_{\text{ATIR}} \cdot \boldsymbol{E}. \tag{11}$$

The corresponding Jones matrix is

$$T_{\text{ATIR}} = \begin{bmatrix} \hat{r}_p & 0 \\ 0 & \hat{r}_s \end{bmatrix}, \tag{12}$$

and $\hat{r}_p$, $\hat{r}_s$ are the amplitude coefficients of reflection for the ATIR field [8].

The coherence matrices $\boldsymbol{J}$,$\boldsymbol{J}'$of the fields, measured in the entrance and

exit pupils of the ATIR prism, respectively, are related by $\boldsymbol{J}' = (\boldsymbol{T}_{\mathrm{ATIR}} \times \boldsymbol{T}^{*}_{\mathrm{ATIR}})$, where $\times$ means the outer product.

The Stokes vector $\boldsymbol{S}(S_0,S_1,S_2,S_3)$ of the incident field $\boldsymbol{E}$, defined as

$$\boldsymbol{S} = \begin{bmatrix} S_0 \\ S_1 \\ S_2 \\ S_3 \end{bmatrix} = \boldsymbol{A} \cdot \boldsymbol{J} = \begin{bmatrix} 1 & 0 & 0 & 1 \\ 1 & 0 & 0 & -1 \\ 0 & 1 & 1 & 0 \\ 0 & -i & i & 0 \end{bmatrix} \begin{bmatrix} J_{xx} \\ J_{xy} \\ J_{yx} \\ J_{yy} \end{bmatrix} = \begin{bmatrix} J_{xx} + J_{yy} \\ J_{xx} - J_{yy} \\ J_{xy} + J_{yx} \\ i\left(J_{yx} - J_{xy}\right) \end{bmatrix}$$

is related to the Stokes vector of the ATIR field $\boldsymbol{S}'(S_0',S_1',S_2',S_3')$ by [27, 28]

$$\boldsymbol{S}' = \boldsymbol{M}_{\mathrm{ATIR}} \cdot \boldsymbol{S} \,, \tag{13}$$

where the Mueller matrix for ATIR is defined as

$$\boldsymbol{M}_{\mathrm{ATIR}} = \boldsymbol{A} \cdot (\boldsymbol{T}_{\mathrm{ATIR}} \times \boldsymbol{T}^{*}_{\mathrm{ATIR}}) \cdot \boldsymbol{A}^{-1}.$$

This matrix has the form [6]

$$\boldsymbol{M}_{\mathrm{ATIR}} = \begin{bmatrix} m_{11} & m_{12} & 0 & 0 \\ m_{21} & m_{22} & 0 & 0 \\ 0 & 0 & m_{33} & m_{34} \\ 0 & 0 & m_{43} & m_{44} \end{bmatrix}, \tag{14}$$

and the matrix elements are

$$\begin{aligned} m_{11} = m_{22} &= \frac{1}{2}\left(\hat{r}_p^{*}\hat{r}_p + \hat{r}_s^{*}\hat{r}_s\right), \quad m_{12} = m_{21} = \frac{1}{2}\left(\hat{r}_p^{*}\hat{r}_p - \hat{r}_s^{*}\hat{r}_s\right), \\ m_{33} = m_{44} &= \frac{1}{2}\left(\hat{r}_p^{*}\hat{r}_s + \hat{r}_s^{*}\hat{r}_p\right), \quad m_{34} = m_{43} = \frac{1}{2} i\left(\hat{r}_p^{*}\hat{r}_{ps} - \hat{r}_s^{*}\hat{r}_p\right). \end{aligned} \tag{15}$$

The complex reflectivities $\hat{r}_p$, $\hat{r}_s$ are functions of the angle of incidence, the optical properties of all media, the light is passing through, the optical properties of the attenuating media and the gap width h. So the Stokes vector of the exit ATIR field $\boldsymbol{S}'\left(S_0', S_1', S_2', S_3'\right)$ is also a function of all these quantities. It also depends on the state of polarization of the input light.

Now the interferometric signal detected by the photodiode array can by expressed in terms of the polarization state of the ATIR wave. Denoting by $\boldsymbol{x},\boldsymbol{y}$ the corresponding unit vectors, the complex amplitude in the exit of the PBS is

$$\boldsymbol{E}'' = E_p'' \boldsymbol{x} + E_s'' \boldsymbol{y} = \boldsymbol{E}_p + \boldsymbol{E}_s \,, \tag{16}$$

where

$$E_p^{''} = E_p^{'} \exp\left\{-\mathrm{i}\left[(\omega t - \varphi_0) - \left(\boldsymbol{k}_p \boldsymbol{r} + \frac{2\pi}{\lambda} n_o L\right)\right]\right\},$$

$$E_s^{''} = E_s^{'} \exp\left\{-\mathrm{i}\left[(\omega t - \varphi_0) - \left[\boldsymbol{k}_s \boldsymbol{r} + \frac{2\pi}{\lambda}\left(d_1(x) n_o + \frac{L - d_1(x)}{\cos\beta} n_e(\beta)\right)\right]\right]\right\}, \qquad (17)$$

$d(x)$ is the current thickness of the second right angle prism of the Rochon PBS; $\boldsymbol{r}$ is the radius vector of the point of measurement that lays on the linear array photo detector. It is placed along the *x* axes of the *Oxz* plane; $\boldsymbol{k}_p$,$\boldsymbol{k}_s$ are the wave vectors of the ordinary and extraordinary waves, corresponding to the *p*- and *s*-components of the ATIR field, respectively;β is the angular shear introduced by the Rochon PBS, *L* is the *x*-length the Rochon prism.

Here we denoted the complex amplitudes of the ATIR field by

$$E_p^{'} = E_p \hat{r}_p \ ,$$

$$E_s^{'} = E_s \hat{r}_s \ . \qquad (18)$$

If the direction of transmission *pp´* of the analyzer A has an azimuth *g* measured from the *x* axes, the field in the exit pupil of the interferometer is

$$\boldsymbol{E}_{\mathrm{pp}^{'}} = \boldsymbol{E}_{\mathrm{p}} \cos\gamma + \boldsymbol{E}_{\mathrm{s}} \sin\gamma \ . \qquad (19)$$

Here we suppose that the exit pupil of the interferometer coincides with the entrance pupil of the detector (no geometrical effects of vignetting take place). The elements of the coherence matrix $\boldsymbol{J}^{''}$ in the exit pupil of the PBS are

$$\left\langle E_x^{''*} E_x^{''} \right\rangle = \left\langle E_x^{''*} E_x^{'} \right\rangle = J_{xx}^{'} = \frac{1}{2}\left(S_0^{'} + S_1^{'}\right) \ ,$$

$$\left\langle E_y^{''*} E_y^{''} \right\rangle = \left\langle E_y^{''*} E_y^{'} \right\rangle = J_{yy}^{'} = \frac{1}{2}\left(S_0^{'} - S_1^{'}\right) \ ,$$

$$\left\langle E_x^{''*} E_y^{''} \right\rangle = \left\langle E_x^{'*} E_y^{'} \right\rangle \exp\left[-i\Delta\right] = J_{xy}^{'} \exp\left[-i\Delta\right] = \frac{1}{2}\left(S_2^{'} + iS_3^{'}\right) \exp\left[-i\Delta\right],$$

$$\left\langle E_y^{''*} E_x^{''} \right\rangle = \left\langle E_y^{'*} E_x^{'} \right\rangle \exp\left[i\Delta\right] = J_{yx}^{'} \exp\left[i\Delta\right] = \frac{1}{2}\left(S_2^{'} + iS_3^{'}\right) \exp\left[i\Delta\right], \qquad (20)$$

where $\Delta = (\boldsymbol{k}_p - \boldsymbol{k}_s)\boldsymbol{r} + \frac{2\pi}{\lambda} d_2(x)\left[n_o - \frac{n_e(\beta)}{\cos\beta}\right]$.

The intensity of the field, falling on the detector is given by the autocorrelation $I(\boldsymbol{r}) = J_{pp'}$.

Then, substituting from (10) and (11) we can write for the output intensity distribution

$$I(\boldsymbol{r}) = J'_{xx}\cos^2\gamma + J'_{yy}\sin\gamma + \left\{J'_{xy}\exp[-i\Delta] + J'_{yx}\exp[i\Delta]\right\}, \tag{21}$$

or expressed by the Stokes parameters of the ATIR field, the measured intensity is

$$I(\boldsymbol{r}) = \frac{1}{2}\left[S'_0 + S'_1\cos 2\gamma + (S'_2\cos\Delta + S'_3\sin\Delta)\sin 2\gamma\right]. \tag{22}$$

This formula allows us to determine the intensity of the interferometrical signal in any point $\boldsymbol{r}$ as a function of the gap width h for known optical constants of all media, the light is passing through, and predefined parameters of the interferometer.

A numerical model of (22) was realized for silicon attenuator (n = 3.85 – i0.02 for λ = 0.6329 μm [10]) and angular shear β = 0.0002205 rad. The detector aperture, placed along the x axes, is supposed to be 14 mm long, which is approximately the length of the array detector used for the measurements. The input wave is linearly polarized at +45° according x axes. The process of evolution of the Stokes parameters is shown in Fig. 6. In Fig. 6 a is shown the trajectory of the Stokes vector on the Poincare sphere and in Fig. 6b is the evolution of the Stokes parameters as a function of the separation h. The interference fringes intensity topography is shown in Fig. 7a. In Fig. 7b is shown the contour plot of the same intensity distribution as a function of the gap width h and the detector aperture coordinate x.

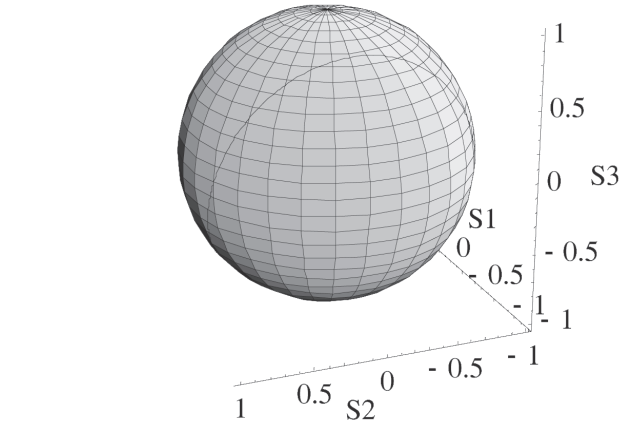

a

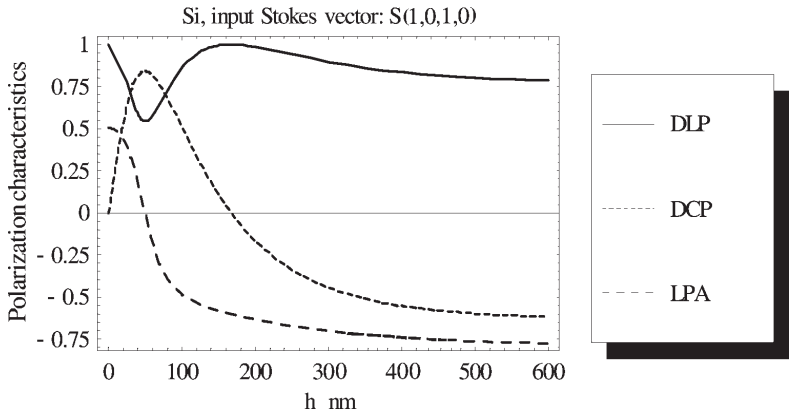

b

Fig. 6. The trajectory of the Stokes vector on the Poincare sphere (a);
b) the Stokes parameters evolution as a function of the gap width *h* for Si attenuator and input Stokes vector *S*(1,0,1,0). DLP – degree of linear polarization, DCP – degree of circular polarization, LPA – linear polarization azimuth

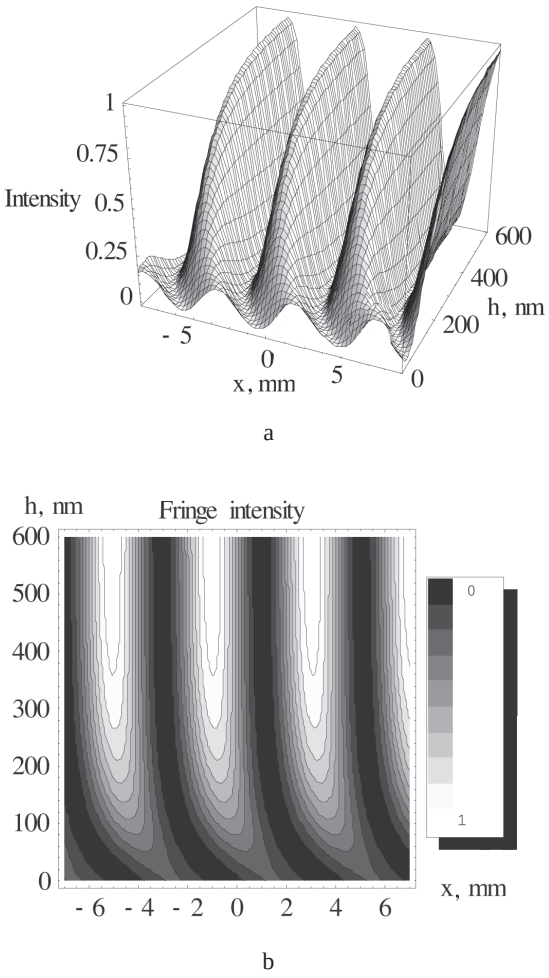

Fig. 7. The theoretical fringe intensity distribution: a) the topography, b) the contour plot. Both plots as a function of the gap width *h* and the detector coordinate *x*

3.2 EXPERIMENT

In this experiment we use the same elements and conditions as in Section 2. In addition we used a λ/2-plate (Carl Zeiss, Jena) to adjust the azimuth of the input linearly polarized wave at +45° according *x* axes. The right angle prism was made of BK10 optical glass and works in TIR. The polarization interferometer consists of a Rochon prism, playing the role of a polarizing beam splitter and a linear polarizer mounted in an angular scale with nonius allowing readings of 0.1 deg. As a detector of the fringe intensity distribution

a photodiode array (Matsushita, model MN-512K) with 512 elements was used. Each fringe intensity distribution showed in Fig. 8 is an average of twenty measurements. The scanning time for each reading was programmed between 4 and 16 ms.The angle of incidence θ was adjusted as 45°.

In this experiment, the attenuating media was a small sample of a bulk optically polished plate of silicon mono-crystal, N-type, cut at [1,0,0] (n = 3.85 – i0.02 for λ = 0.6329 μm [10]). The gap width h was controlled by an external (not shown on the figure) interferometer that follows the white light Fizeau fringes, observed in direction normal to the hypotenuse of the TIR prism. The fringe intensity distribution along the detector aperture for three values of the gap width h is shown in Fig. 8.

Following the fringe maxima intensity, for example of the second fringe from the left side of Fig. 8, as a function of the increasing value of the separation h, we observe a monotonous shift of the fringe to the left and simultaneous rise of the intensity. There is some agreement between this phenomena and the theoretical prediction, shown in Fig. 7. The intensity curves in Fig. 8 are actually slices of the intensity topography, shown in Fig. 7 for discrete values of h. The measured values (Fig. 8) of the lateral shifts for separations h = 85 nm and h = 120 nm are grater than the theoretical. The source of this discrepancy is probably the limited precision of the visual two-beam interferometrical method, used for the gap width measurements. The dynamics in the form and topology of the interference fringes was proved by a series of measurements for different values of the gap width. Not only

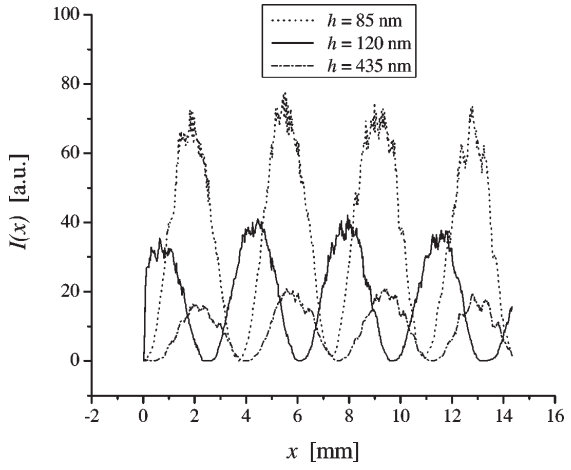

Fig. 8. The interference fringes intensity, obtained with Si attenuator, as a function of the photodiode array coordinate x, for three values of the gap width: dashed line h = 435 nm, solid line h = 120 nm, dot line h = 85 nm

a lateral shift of the fringe system (along the x axes) is observed but also a saddle like variations of the intensity. The measurements proved that the fringe parameters are stable for values of $h > 400$ nm (approximately $\lambda/2$), which is in agreement with the theory (Fig. 7a,b). But for separations $h < \lambda/2$, the intensity of the signal decreases and the whole pattern shifts laterally. The cause for these effects is the intensive variations of the Stokes parameters of the ATIR field (see Fig. 6) when the value of the gap width h increases monotonically from zero.

4. CONCLUSION

The interferometer here described proved to be a successful instrument for ATIR phase investigation. The experiments gave results in good agreement with theory. An additional analysis of fringe contrast will improve the accuracy of the method of phase shift determination. A refinement of the h-displacement technique will allow a detailed study of the ATIR caused by metals, semiconductors, and other media. For example, calculations showed that bulk Al exhibits linear dependence between Δ and h. The method can be used not only in the research, but in other applications, such as h-displacement measurements for the purposes of the sensor technique, surface relief testing, contamination monitoring, refractometry of absorbing media, etc.

The here described example is a good demonstration of the significance of the evolution of the polarization state of the ATIR wave, caused by variations of the value of the gap width and the optical properties of all media participating the process of ATIR.

The experimental measurements lead us to the necessity of an analysis of the phase-amplitude dependences in the process of ATIR. From Fig. 6. is seen that when the separation h decreases to zero, the output field passes through great variety of polarization states. Starting in approximately linear polarization state (for $h = 0$), the increasing separation h drives the ATIR field up in the space of the right polarizations. The trajectory of the Stokes vector passes near the “north pole” (right polarized elliptical wave with low eccentricity) of the Poincare sphere and goes “down to south” to the elliptical states with still higher eccentricity, penetrates the equator (linear state) and continues in the space of the left polarized elliptical states. The inclination of the polarization ellipses during this process is varying as well. The limit point of the trajectory is a left elliptical polarization corresponding to that of pure TIR. The interferometer combines the amplitudes and the phases of two orthogonal components (x and y in the chosen coordinate system) of this field. This leads to a theoretical prediction of the intensity distribution of the interference

fringes (Fig. 7), which shows variations in the intensity and continuous shift of the interference fringes to the right for decreasing *h*. A comparison with the experimental results (Fig. 8) obtained with silicon attenuator exhibits an agreement between theory and experiment.

The numerical comparison of the Stokes parameters evolution for silicon and tantalum (at the same other conditions) showed the significance of the weight distribution of the value of the complex index of refraction between its components: the index of refraction *n* and the extinction coefficient *k*. If the value of *k* increases and that of *n* decreases two effects are observed: a saddle in the intensity profile for gap widths $h < 200$ nm and strong and progressive lateral shift of the fringes. The common conclusion is that higher values of the extinction coefficient lead to higher nonlinearity of the output interferometrical signal as a function of the separation *h*, especially for gap widths $h < 200$ nm.

The form of the output signal is also highly dependant on the value of the Stokes vector of the input wave. In this work we considered theoretically and used in the measurements a monochromatic wave linearly polarized at +45°.

The aforementioned results will be possibly of practical interest in the development of newer methods for absorption measurements or surface relief sensing.

Acknowledgments: This work was supported by the National Fund of Scientific Research of Bulgaria, grant No. VUF 02/05.

REFERENCES

1. Kan'an, A.M., and R.M.A. Azzam. *Opt. Engineering*, **33**, 1994, 2029.
2. Spiller, E. *Appl. Optics*., **23**, 1984, 3544.
3. Cojocaru, E. *Appl. Optics*, **33**, 1994, 7425.
4. Wang, Yu. *Appl. Phys. Lett.*, **67**, 1995, 2759.
5. Li, H., and Sh. Xie. *Appl. Optics*, **35**, 1996, 1793.
6. Spiller, E. *Appl. Optics*, **23**, 1984, 3544.
7. Heinzelmann, H., and D.W. Pohl. *Appl. Phys. A*, **59**, 1994, 89.
8. Culshow, W. *Appl. Optics*, **11**, 1972, 2639.
9. Knittl, Z. Optics of thin films, NY, 1976.
10. Azzam, R. M. A. *Appl. Optics*, **24**, 1985, 513.
11. Culshow, W., and D.S. Jones. *Proc. Phys. Soc.*, **B66**, 1953, 859.
12. Born, M., and E. Wolf. Principals of Optics, London, 1959.
13. Shurcliff, W.A. Polarized Light, Harvard UP, 1966.
14. Sainov, S., and O. Tonchev. *Optics and Lasers in Eng.*, **10**, 1989, 17.
15. Sainov, S., and O. Tonchev. *Optics and Lasers in Eng.*, **15**, 1991, 267.
16. Nakadate, S. *J. Opt. Soc. Am*. A, **5**, 1988, 1258.
17. Nakadate, S. *J. Opt. Soc. Am*. A, **5**, 1988, 1265.
18. Nakadate, S. *Appl. Optics*, **29**, 1990, 242.

19. Steel, W.H., Interferometry, Cambridge UP, 1967.
20. Malacara, D. Optical Shop Testing, NY, 1978.
21. Bennett, J.M., and H.E. Bennett. in Handbook of Optics, McGraw-Hill, 1978.
22. Stoyanov, H.Y. *Optics and laser technology*, **32**, 2000, 147.
23. Thompson, A.R., J.M. Morgan, and G.W. Swenson. Interferometry and synthesis in radio astronomy, NY, 1986.
24. Beckman, V.Yu. *Technical Physics*, **44**, 1999, 1103.
25. Schafers, F. *Appl. Optics*, **38**, 1999, 4074.
26. Collett, Ed. *Am. J. Phys.*, **36**, 1968, 713.
27. Marathay, A.S. *J. Opt. Soc. Am.*, **55**, 1965, 969.
28. Marathay, A.S., *J. Opt. Soc. Am.*, **56**, 1966, 619.
29. Svirco, Yu., and N. Zheludev. Polarization of Light in Nonlinear Optics, NY, 1998.
30. Brausseau, Ch. *Opt. Letters*, **20**, 1995, 1221.
31. Bueno, J. M. *J. Opt. A: Pure Appl. Opt.*, **2**, 2000, 216.
32. Landolt-Börnstein, Band II, 8 Teil, Optishe Konstanten, Heidelberg, 1967.

Received November 2005

Hristiyan Y. Stoyanov
St. Kliment Ohridski, University of Sofia
Faculty of Physics
Department of Quantum Electronics
5 James Bourchier Buld,
Sofia 1164, Bulgaria
E-mail: hystoy@phys.uni-sofia.bg